Polymer 52 (2011) 2947–2955

Contents lists available at ScienceDirect

Polymer

journal homepage: www.elsevier.com/locate/polymer

Magnetic polyacrylonitrile-Fe@FeO nanocomposite fibers - Electrospinning, stabilization and carbonization

Jiahua Zhu [a], Suying Wei [b], Dan Rutman [a], Neel Haldolaarachchige [c], David P. Young [c], Zhanhu Guo [a,*]

[a] Integrated Composites Laboratory (ICL), Dan F. Smith Department of Chemical Engineering, Lamar University, Beaumont, TX 77710, USA
[b] Department of Chemistry and Biochemistry, Lamar University, Beaumont, TX 77710, USA
[c] Department of Physics and Astronomy, Louisiana State University, Baton Rouge, LA 70803, USA

ARTICLE INFO

Article history:
Received 22 March 2011
Received in revised form
10 April 2011
Accepted 16 April 2011
Available online 23 April 2011

Keywords:
Magnetic carbon nanocomposite fibers
Polyacrylonitrile
Iron nanoparticles

ABSTRACT

Uniform and bead-free pure polyacrylonitrile (PAN) and its magnetic polymer nanocomposite (PNC) fibers reinforced with different core-shell Fe@FeO nanoparticles (NPs) loadings are prepared using electrospinning method. The morphology of the resulting products is correlated to the corresponding rheological behaviors of the pure PAN and PAN/Fe@FeO solutions. The diameter of the PAN fibers is linearly related to the polymer solution concentration. However, with a fixed PAN concentration of 10 wt %, the Fe@FeO NP loading shows a negligible effect on the morphology of the PNC fibers. Thermogravimetric analysis (TGA) results indicate an enhanced thermal stability of the PNC fibers than that of the pure PAN fibers. Magnetic carbon nanocomposite (MCNC) fibers are prepared through the stabilization and carbonization of the electrospun PNC fibers. The effects of the heating procedures, including the stabilization and carbonization temperature and time, on the fiber morphology are systematically investigated. Both short and long MCNC fibers could be easily produced by changing the heat procedures. Room temperature magnetic properties of the nanocomposite fibers based on different heating procedures are also studied in this work.

1. Introduction

Owing to its comparatively low-cost manufacturing and easy deployment even on a laboratory bench, electrospinning technology has launched polymer micro- and nano- fibers, and broadens the realms of nanotechnology and materials science [1]. Although the most commonly studied material is polymer, electrospinning has been used to prepare continuous fibers from a huge range of materials, such as composites [2–4], semiconductors [5] and ceramics [6,7]. Electrospun fibers, especially in the nanoscale, have found applications in various fields. For example, electrospun polymer nanofibers possessing high porosity and large specific surface area (surface-to-volume ratio) have been used as membranes for gas separation, protein purification, and waste water treatment [8–10]. However, there are still some challenges for the long-term usage of these polymer fibers, such as the inferior thermal stability of the pure polymers [11], low mechanical strength, and solvent absorption (swelling effect) when exposed to liquids or gases [12]. Polymers reinforced with inorganic materials have been demonstrated to be an effective way to enhance the thermal, mechanical and other physical properties of the polymers [13–18].

Carbon fibers are widely investigated due to their extremely high mechanical strength and modulus, excellent thermal and electrical conductivities. Therefore, they are widely used as large load-bearing composites [19], super-capacitors [20,21], filters [22] and catalyst supports for the rechargeable batteries or fuel cells [23,24]. Conventionally, carbon fibers are prepared from polyacrylonitrile (PAN) or pitch precursors [25,26] and the typical diameter ranging from 5 to 10 μm. Chemical vapor deposition (CVD) method has been investigated to produce carbon fibers in nanosize diameter. However, the complicated physical and chemical processes associated with the high manufacturing cost have always been the major hurdle for large-scale applications. The rapidly developed electrospinning technology provides a flexible and cost-effective way to produce carbon fibers with diameter ranging from micro- to nano- meters [20]. In addition, the electrospinning approach is especially useful in fabricating continuous aligned carbon fibers with desired length, which depend on the spinneret geometry [27] and thermal treatment including the stabilization and carbonization. Recently, ceramic fibers of alumina-borate [28], titania [7], silica [29], niobium oxide [30] and copper oxide [31] are also produced using electrospinning

* Corresponding author. Tel.: +1 409 880 7654.
E-mail address: zhanhu.guo@lamar.edu (Z. Guo).

0032-3861/$ – see front matter © 2011 Elsevier Ltd. All rights reserved.
doi:10.1016/j.polymer.2011.04.034

technology. Incorporating nanoparticles (NPs) in the carbon fibers is of great interest due to the combined advantages of the two phase materials, such as the unique catalytic, optical, magnetic properties of the nanomaterials and the excellent thermal stability, chemical inertness, high mechanical strength of the carbon fibers. Steigerwalt et al. [24] introduced a decomposition method to prepare the Pt-Ru/carbon nanocomposite fibers with an aim to enhance the anode catalyst performance of the direct methanol fuel cells (DMFC). Even though an enhancement of 64% is observed in the nanocomposite fibers as compared to that of the unsupported Pt-Ru colloids, the repeatability of the catalysis performance is not discussed, which is actually very important considering the bonding strength between the NPs and the carbon fiber surface. Electrospinning is able to produce carbon nanocomposite fibers with strong interaction between the NPs and the fiber matrix through embedding the NPs within the fibers [4]. Carbon fibers with a specific functionality would definitely trigger further interest in the structural materials, catalytic and sensing applications. Electrospun PAN fibers and the corresponding carbon fibers have been well investigated in the last two decades. However, less work has been done on fabricating PAN based nanocomposite fibers to achieve the multi-functionalities.

In this paper, uniform and bead-free electrospun magnetic PAN-based nanocomposite fibers and the corresponding magnetic carbon-based nanocomposite fibers after stabilization and carbonization are reported. The polymer concentration effects on the resulting PAN fiber diameter together with the effects of the heat treatment history including stabilization and carbonization (temperature and time) on the magnetic carbon nanocomposite fiber morphology are investigated. The thermal history has a significant effect on the length of the resulting magnetic carbon nanocomposite fibers. Compared to the magnetic PAN nanocomposite fibers, the magnetic carbon nanocomposite fibers are magnetically softer with an observed decreased coercivity, while the saturated magnetization increased in different scale depending on the thermal processes.

2. Experimental

2.1. Materials

Polyacrylonitrile (PAN, $M_w = 150{,}000$, $X_n = 283$ and the density is 1.184 g/cm^3) was purchased from Scientific Polymer Products Inc. Anhydrous N, N-dimethylformamide (DMF, 99.9%) was commercially available from Alfa Aesar. Core@shell structured Fe@FeO NPs with a particle size of 15–25 nm and an oxide thickness of 0.5 nm, were provided by QuantumSphere, Inc. All the materials were used as-received without any further treatment.

2.2. Preparation of pure polyacrylonitrile fibers

The PAN/DMF solutions were prepared by magnetic stirring at room temperature with a polymer loading of 8, 10, 12 and 14 wt%, respectively. Pure PAN fibers were prepared using an electrospinning method. Typically, a 10-ml syringe with a stainless steel gauge needle (inner diameter, 0.80 mm) was used to load the polymer solution. A high-voltage power supply (Gamma High Voltage Research, Product HV power Supply, Model No. ES3UP-5w/DAM) was used and connected to the stainless needle. The grounded counter electrode was a flat aluminum foil. The polymer solution was constantly and continuously supplied by a syringe pump (NE-300, New Era Pump System, Inc.). The applying voltage, volume feed rate and tip-to-collector distance were 20 kV, 10 μl/min and 15 cm, respectively.

2.3. Preparation of polymer nanocomposite fibers

The specific weight of the NPs, calculated based on pure PAN and NPs, was mixed with 10 wt% PAN/DMF solution to achieve various Fe@FeO loadings (1, 3, 7 and 10 wt %). The Fe@FeO NPs were dispersed in the PAN/DMF solution by ultrasonication at room temperature for 90 min. The PNC fibers were electrospun using the same aforementioned setup with an applied voltage to 25 kV. The higher voltage was introduced to overcome the increased viscoelastic force with the addition of the NPs. The feed rate and tip-to-collector distance retained the same as 10 μl/min and 15 cm as used for electrospinning the pure PAN fibers. Both pure PAN and PAN/Fe@FeO PNC fibers were dried in a vacuum oven to remove the solvent residue at room temperature and stored for further characterizations and thermal treatment.

2.4. Preparation of carbon nanocomposite fibers

The polymer fibers were converted to carbon fibers after the thermal stabilization and carbonization in a Lindberg Blue M tube furnace (Thermo Scientific Inc, maximum temperature: 1100 °C). The carbon fibers produced from different heat treatment were designated as CF1, MCF2, MCF3, MCF4, MCF5 and MCF6, respectively. CF1 represents carbon fibers made from pure PAN fibers. The other five samples from MCF2 to MCF6 were the magnetic carbon nanocomposite fibers made from the PNC fibers with a Fe@FeO particle loading of 10 wt% after different heating procedures. The detailed heating procedures are summarized, Table 1.

2.5. Characterization

The rheological behaviors of the pure PAN and PAN/Fe@FeO PNC DMF solutions were investigated with an AR 2000ex Rheometer (TA Instrumental Company) at shear rate ranging from 1 to 1200 rad/s at 25 °C. A series of measurements were performed in a cone-and-plate geometry with a diameter of 40 mm and a truncation of 66 μm.

Fourier transform infrared spectroscopy (FTIR, Bruker Inc. Tensor 27) with hyperion 1000 ATR microscopy accessory was used to characterize PAN and PAN/Fe@FeO PNC fibers over the range of 4000–500 cm^{-1} at a resolution of 4 cm^{-1}.

Table 1
Thermal history of the stabilization and carbonization processes.

Name	Heat procedures
CF1(pure)	$25^\circ C \rightarrow^{1h}_{Air} 280^\circ C \rightarrow^{3.5h}_{Air} 280^\circ C \rightarrow^{3.5h}_{N_2} 700^\circ C \rightarrow^{2h}_{N_2} 700^\circ C \rightarrow^{\text{Naturally cooling}}_{N_2} 25^\circ C$
MCF2	$25^\circ C \rightarrow^{1h}_{Air} 280^\circ C \rightarrow^{3.5h}_{Air} 280^\circ C \rightarrow^{3.5h}_{N_2} 700^\circ C \rightarrow^{2h}_{N_2} 700^\circ C \rightarrow^{\text{Naturally cooling}}_{N_2} 25^\circ C$
MCF3	$25^\circ C \rightarrow^{2h}_{Air} 250^\circ C \rightarrow^{1h}_{Air} 250^\circ C \rightarrow^{2h}_{N_2} 600^\circ C \rightarrow^{1h}_{N_2} 600^\circ C \rightarrow^{5h}_{N_2} 25^\circ C$
MCF4	$25^\circ C \rightarrow^{2h}_{Air} 250^\circ C \rightarrow^{1h}_{Air} 250^\circ C \rightarrow^{2h}_{N_2} 800^\circ C \rightarrow^{1h}_{N_2} 800^\circ C \rightarrow^{5h}_{N_2} 25^\circ C$
MCF5	$25^\circ C \rightarrow^{2h}_{Air} 300^\circ C \rightarrow^{2h}_{Air} 300^\circ C \rightarrow^{2h}_{N_2} 800^\circ C \rightarrow^{1h}_{N_2} 800^\circ C \rightarrow^{5h}_{N_2} 25^\circ C$
MCF6	$25^\circ C \rightarrow^{2h}_{Air} 300^\circ C \rightarrow^{2h}_{Air} 300^\circ C \rightarrow^{2h}_{N_2} 800^\circ C \rightarrow^{8h}_{N_2} 800^\circ C \rightarrow^{5h}_{N_2} 25^\circ C$

The morphologies of the pure PAN and PAN/Fe@FeO nanocomposite fibers were obtained using scanning electron microscopy (Hitachi S-3400 scanning electron microscopy). All samples were sputter coated with a thin gold layer (Penton Mark IV) to improve the conductivity for a better imaging quality.

The thermal stability of the pure PAN and PAN/Fe@FeO PNC fibers was studied by a thermal gravimetric analysis (TGA, TA Instruments Q500) under a heating rate of 10 °C/min and an air flow rate of 60 ml/min from 25 to 700 °C. Differential scanning calorimetry (DSC, TA Instruments Q2000) measurements were carried out under a nitrogen flow rate of approximately 10 cm^3/min at a heating rate of 20 °C/min from 50 to 350 °C.

The magnetic properties of the magnetic carbon fibers and the electrospun PNC fibers at room temperature were recorded in a 9T physical properties measurement system (PPMS) by Quantum Design.

3. Results and discussion

3.1. Rheological behaviors

Fig. 1 shows the viscosity and shear stress as a function of shear rate for the PAN/DMF solution (PAN loading: 8 and 10 wt%) and the Fe@FeO NPs suspended PNC/DMF solutions (NP loading: 1, 3 and 7 wt%). Shear thinning (viscosity decreases with an increase of the shear rate/frequency) is observed in all the solutions [32,33]. The viscosity and shear stress of the 10 wt% PAN/DMF solution are almost doubled the values observed in the 8 wt% PAN/DMF solution. The viscosity curves of the PNC/DMF solutions seem overlapped at low shear rate and the difference becomes larger with increasing shear rate, where the viscosity is positively proportional to the nanoparticle loadings. It is worth noticing that the 1 wt% Fe@FeO PNC solution shows sharper shear thinning as compared to the pure PAN solution, and thus a crossover point at the shear rate of 600 l/s is observed between these two curves. At lower shear rates (<600 l/s), the polymer chain segmental motion is greatly restricted by the NPs due to the well known "confinement effect" [34]. Therefore, the PNC solutions show higher viscosity as compared to the pure PAN solution. However, as the shear rate exceeds 600 l/s, the 1 wt% Fe@FeO PAN/DMF solution shows even lower viscosity than that of the pure PAN solution. Recently, a reduced viscosity with a better nanofiller dispersion is reported in the fullerene and magnetite NPs/polystyrene PNCs [35] and polystyrene NPs in a linear polystyrene [36]. These reduced viscosity observations are due to the slip and or inhomogeneous flow [35,36]. Similar reduced viscosity is also observed in our previous work of the Fe_3O_4 NPs suspended in polyacrylonitrile DMF solutions, which is interpreted in terms of the enhanced orientated polymer chains [37]. The NPs introduced into the polymer solution will definitely bring the inhomogeneity and enhance the polymer chain orientation. Thus, a decreased viscosity is observed.

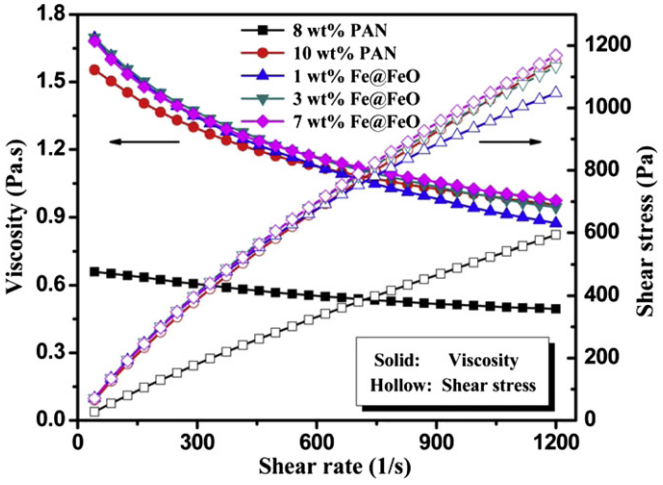

Fig. 1. Viscosity and shear stress vs shear rate of the PAN-DMF solutions and the Fe@FeO NPs suspended PAN/DMF solutions. The NPs suspended solutions are based on 10 wt% PAN.

The rheology of a non-newtonian fluid is often described by power law equation, Eq. (1):

$$\tau = K\ \dot{\gamma}^n \tag{1}$$

where τ is the shear stress, K is the flow consistency index, $\dot{\gamma}$ is the shear rate and n is the flow behavior index. The value of the n determines the fluid type. For $n < 1$, pseudoplastic fluids; $n = 1$, Newtonian fluids; $n > 1$, dilatant fluid. The rheological data are summarized in Table 2. The n values for all the samples are less than 1, indicating a pseudoplastic nature of the solutions. With the increase of the PAN concentration, the n value decreases corresponding to a more obvious pseudoplastic behavior. For non-newtonian fluid, the orientation of the polymer chains is the governing factor, that influences the fluid behavior [38]. Thus, the greatly decreased viscosity of the PAN solution at larger shear rate is primarily due to the polymer segments orientation. For the PNC/DMF solution, the gradually increased n value with increasing nanoparticle loadings shows the trend of these solutions approaching Newtonian fluid behavior, Table 2. However, the highest value $n = 0.82$ observed in the 7 wt% Fe@FeO solution is still slightly lower than $n = 0.83$ observed in the pure PAN solution, indicating a more pseudoplastic behavior of the PNC solution. The flow consistency index K and R^2 are also presented in Table 2.

3.2. Microstructures of the as-spun pure PAN fibers

Fig. 2 shows the SEM microstructures of the pure PAN fibers electrospun from the solutions with a PAN loading of 8, 10, 12 and 14 wt%, respectively. The fibers produced from all the polymer loadings are well separated from each other and no beads are observed. All the fibers show uniform diameter distribution with a polymer loading of 10, 12 and 14 wt%. Except the one with a polymer loading of 8 wt%, the fiber diameter can be roughly divided into two groups with different sizes, Fig. 2a. The appearance of a bimodal diameter distribution of the fibers is due to the splitting of the electrospinning jets during the fiber production. This observation is quite consistent with the results obtained from poly(ethylene oxide) (PEO)/water solution [39] and polyimide/DMF solution [15]. In addition, all the fibers are well separated from each other without any bundles or junctions. This indicates an appropriate tip-to-collector distance (15 cm) in this study, which is long enough to allow the solvent evaporation before reaching the target collector. Polymer concentration is recognized as a key factor influencing the final fiber morphology [40]. An appropriate polymer concentration is necessary to obtain uniform fibers. Generally, extremely high polymer concentration may lead to the

Table 2
The rheological data of the PAN and Fe@FeO/PAN/DMF solutions.

Composition*	n	R^2	K
8 wt% PAN/DMF	0.90	0.9989	1.05
10 wt% PAN/DMF	0.83	0.9982	3.20
1 wt% Fe@FeO/PAN/DMF	0.78	0.9945	4.50
3 wt% Fe@FeO/PAN/DMF	0.80	0.9967	4.02
7 wt% Fe@FeO/PAN/DMF	0.82	0.9981	3.66

*For all composite samples, the PAN loading is 10 wt% in DMF.

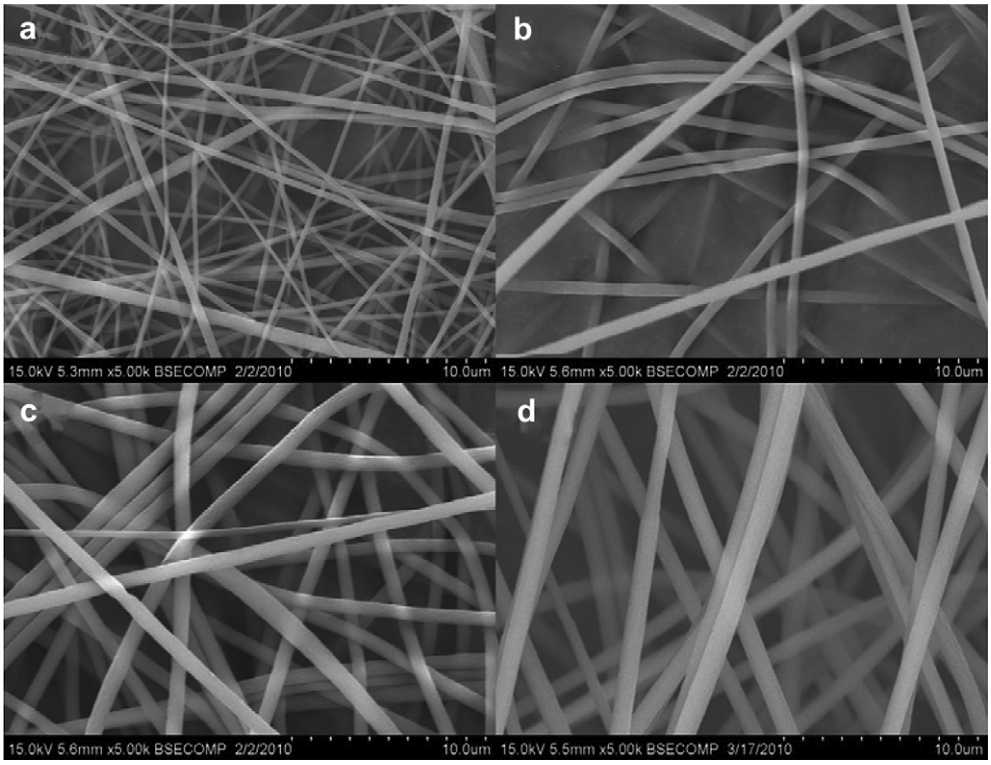

Fig. 2. SEM microstructures of the pure PAN fibers electrospun from the solutions with a polymer loading of (a) 8, (b) 10, (c) 12 and (d) 14 wt%, respectively. Operational parameters: 20 kV, 15 cm and 10 μl/min.

electrospinning process impossible due to the high viscosity, while low concentration usually brings fibers with beads. Our previous study shows that polymer solutions with both 4.0 and 6.5 wt% PAN loading produced the fibers with beads [37]. The fiber morphology is mainly affected by the force balance among the electrostatic repulsion, surface tension and viscoelastic force [41,42] on the liquid drop at the end of the tip. Once the force balance is broken down, the unstable electrospinning jets will result in either beaded fibers or other irregular fibers [39,43].

The average diameter of the electrospun pure PAN fibers as a function of PAN concentration is plotted in Fig. 3. The fiber diameter is observed to be almost linearly related to the PAN concentration. Some other groups tried to construct a relationship between fiber diameter and polymer concentration using a regression method [39,44]. Rather than a linear relationship, they observed a power law relationship with different exponents in regression equation. The various regression equations and exponents suggest the imperfection and complexity of the electrospinning process. The in-flight fiber splitting phenomena is observed in the electrospinning process [45] and this is not always true in the other systems [46], which may be responsible for the complex relationship between the average diameter of the electrospun fibers and the polymer concentration [39]. Besides the polymer concentration, many other factors such as tip-to-collector distance, electrical potential, relative humidity also have significant effects on the diameter of the electrospun fibers [47].

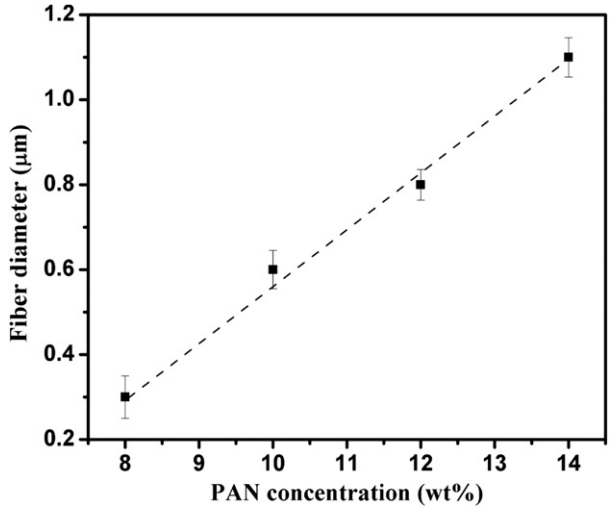

Fig. 3. Average fiber diameter as a function of PAN concentration.

3.3. Electrospun PAN/Fe@FeO PNC fibers

3.3.1. Microstructures of the PNC fibers

Fig. 4 shows the SEM images of the PAN/Fe@FeO PNC fibers with a Fe@FeO nanoparticle loading of 1.0, 3.0, 7.0 and 10.0 wt%, respectively. It is worth noting that the applied voltage was increased to 25 kV for producing uniform PNC fibers to overcome the increased viscoelastic force arising from the more viscous PNC solutions. Similar to the electrospun pure PAN fibers, the fabricated PNC fibers are pretty regular in shape and randomly lied on the collecting electrode. The particle loading shows a negligible influence on the average diameter of the PNC fibers due to the observed similar viscosity in the PNC solutions, Fig. 1. All the fibers electrospun from the solutions with different particle loadings show a similar fiber diameter around 500 nm.

3.3.2. FT-IR analysis

Fig. 5 shows the FT-IR spectra of the as received PAN powder, pure PAN fibers and PNC fibers with different particle loadings,

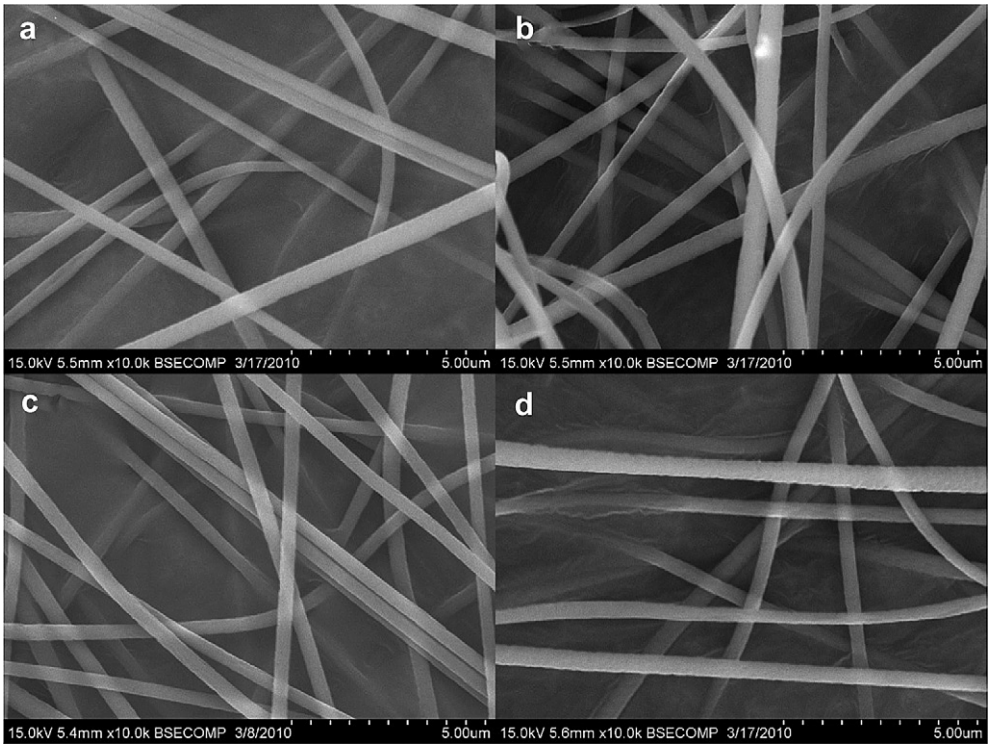

Fig. 4. SEM images of the PAN/Fe@FeO PNC fibers with a particle loading of (a) 1.0, (b) 3.0, (c) 7.0 and (d) 10.0 wt%. Operational parameters: 25 kV, 15 cm and 10 μl/min.

respectively. The peaks at 2940 and 2920 cm^{-1} are due to the stretching vibration of the methylene group (−CH_2−). The strong peak at 2240 cm^{-1} is a characteristic adsorption of the nitriles compound [48] and is assigned to the stretching vibration of the nitriles group (−CN−). The peaks at 1460 and 1360 cm^{-1} are assigned to the bending vibrations of the methylene and methine group [37,49], respectively. The 1250 cm^{-1} peak is due to the wagging vibration of the methine group coupled with the rocking vibration of the methylene group and the 1230 cm^{-1} peak is from the twisting mode of the methylene group coupled with the methine group [50,51]. The 1670 and 1630 cm^{-1} peaks are due to the stretching vibration of the carbon−carbon double bonds present at the end of the polymer chain [52,53]. After comparing the spectra between the pure PAN fibers and PAN/Fe@FeO PNC fibers, no additional new peak is observed, which indicates a physical entanglement rather than chemical interaction between the NPs and the polymer matrix.

3.3.3. TGA analysis

Fig. 6 shows the TGA curves of the pure PAN fibers and the PAN/Fe@FeO PNC fibers. The degradation process of all samples can be roughly divided into three stages, I, II and III. In stage I, all the fibers are thermally stable until the temperature reaches 292 °C. It is worth noting that the weight percentage of the PNC fibers is slightly over 100% between 200 and 300 °C, which is due to the oxidation of the NPs in air. At the very beginning of stage II, all the samples experience a sharp weight loss around 292 °C, which is primarily due to the formation of the ring compounds among −CN groups [54,55]. The NPs exhibit negligible contribution to the

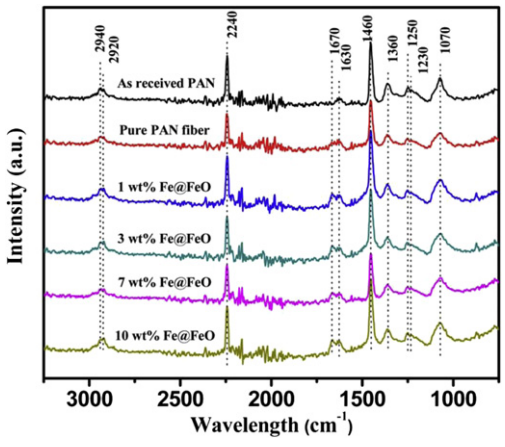

Fig. 5. FT-IR spectra of the as received PAN, pure PAN fibers and PAN/Fe@FeO PNC fibers with different Fe@FeO nanoparticle loadings.

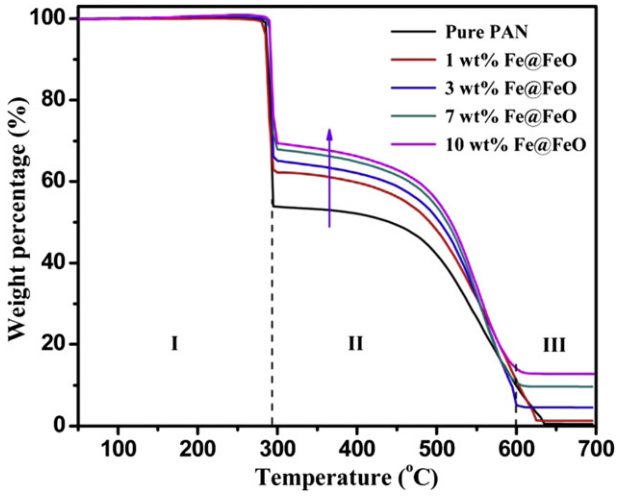

Fig. 6. TGA curves of the electrospun pure PAN fibers and PAN/Fe@FeO PNC fibers.

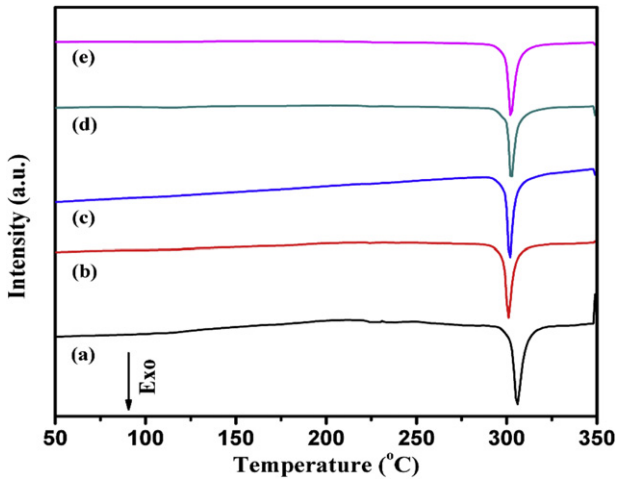

Fig. 7. DSC heating traces of (a) pure PAN fibers and PAN/Fe@FeO PNC fibers with a particle loading of (b) 1, (c) 3, (d) 7 and (e) 10 wt%, respectively.

Table 3
DSC characteristics of the electrospun pure PAN and PAN/Fe@FeO PNC fibers.

Composition	$T_{p\text{-}exo}$ (°C)*	ΔH (J g^{-1})*
Pure PAN	305.5	497.5
1 wt% Fe@FeO	300.9	437.9
3 wt% Fe@FeO	301.6	419.1
7 wt% Fe@FeO	302.6	438.2
10 wt% Fe@FeO	302.4	476.3

*$T_{p\text{-}exo}$: exothermic peak temperature, ΔH: exothermic heat calculated based on pure PAN.

thermal stability of the nanocomposite fibers in this region. However, as the temperature increases to 350 °C, the weight percentage of pure PAN fibers and PAN/Fe@FeO PNC fibers with a particle loading of 1, 3, 7 and 10 wt% are 53.0, 61.5, 64.1, 66.7 and 68.2%, respectively. This thermal stability enhancement is due to the strong interaction between the electronegative –CN groups and the NPs [56]. At the end of stage II, the weight loss curves get close to each other indicating the polymers are almost burnt out. In stage III, typically above 600 °C, the decomposition of the polymer matrix is completed and only the NPs are retained finally. As seen in stage III, the final weight residue of each composition is larger than the initial loading, which is due to the oxidation of the Fe@FeO NPs to Fe_2O_3 during degradation.

3.3.4. DSC characterization

Fig. 7 shows the DSC heating scan curves of the electrospun pure PAN fibers and PAN/Fe@FeO PNC fibers with different particle loadings. The exothermic peak temperature ($T_{p\text{-}exo}$) and exothermic heat enthalpy (ΔH) are summarized in Table 3. The pure PAN fibers show a sharp exothermic peak at 305.5 °C and a slight decrease in $T_{p\text{-}exo}$ is observed in the PNC fibers. The ΔH of the PNC fibers is calculated based on the weight of pure PAN rather than the total weight of the PNCs. The decreased enthalpy value of the PNC fibers than that of the pure PAN fibers indicates the intensified conformational disorder with the addition of the NPs. Being continuously heated to 250–400 °C, the degradation of PAN is explosive in nature, which is attributed to the inefficient removal of the polymerization heat of the nitrile groups, such large amount of heat helps to make a bunch of secondary reactions happen [57]. The samples are then conducted with an additional cooling (350–25 °C) and heating process (25–350 °C again). No obvious peak on the cooling curve is observed and the exothermic peak disappears on the second heating curve (the curve is not shown here). All these results indicate the exothermic reactions occurred during the first heating process, generally

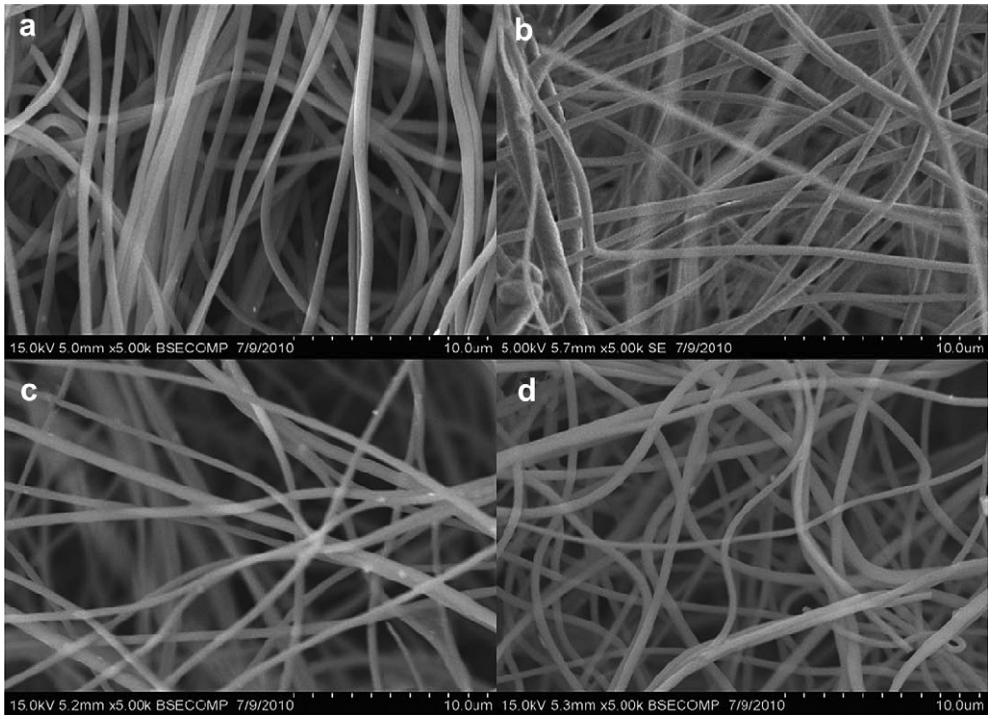

Fig. 8. SEM images of the PAN/Fe@FeO (10 wt%) PNC fibers after 1-h stabilization in air at a temperature of (a) 220, (b) 250, (c) 280 and (d) 300 °C, respectively. Electrospinning operational parameters: 25 kV, 15 cm and 10 μl/min.

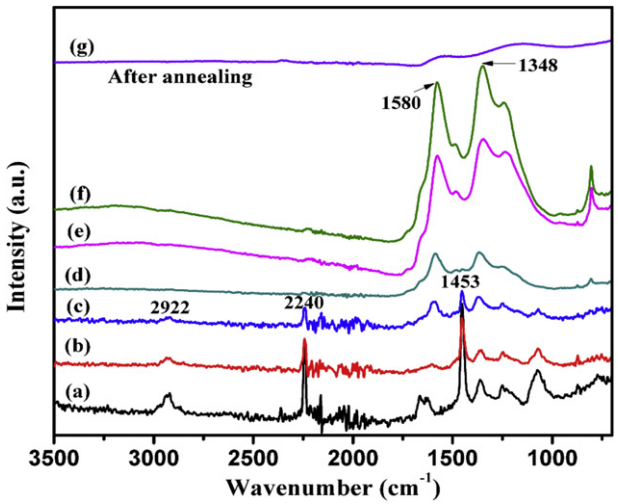

Fig. 9. FT-IR spectra of the PAN/Fe@FeO PNC fibers oxidized in air at a temperature of (a) 25, (b) 200, (c) 220, (d) 250, (e) 280, and (f) 300 °C; and (g) after annealing following the procedure of MCF6 in Table 1.

including the dehydrogenation, instantaneous cyclization and cross-linking reactions [58]. The exothermic peak is regarded as the result of the nuclephilic attack on a nitrile followed by instantaneous cyclization reaction to an extended conjugated structure, which corresponds to the exothermic oxidative stabilization process [59].

3.4. Stabilization of PAN/Fe@FeO PNC fibers

Fig. 8 shows the PAN/Fe@FeO PNC fibers after stabilization under 220, 250, 280 and 300 °C, respectively. The fibers retain their continuity without any breakage after different heat treatments. And it is worth to notice that the fibers are relatively wavy after heating at 280 and 300 °C, Fig. 8c,d than those heated at 220 and 250 °C, Fig. 8a,b. Previous reports on the stabilization of pure PAN indicate that the conjugated polyene structures along the PAN fiber molecules are preliminarily formed to some extent during the prolonged stabilization treatment at 235 °C. Accompanied by the dehydrogenation and/or dehydrocyanide reactions to form the conjugated polyene structures along the backbone chain during stabilization, the more stable ladder structures of PAN fibers are formed [60]. The wavy shaped fibers after heating at higher temperatures are probably due to the unbalanced inner-stress

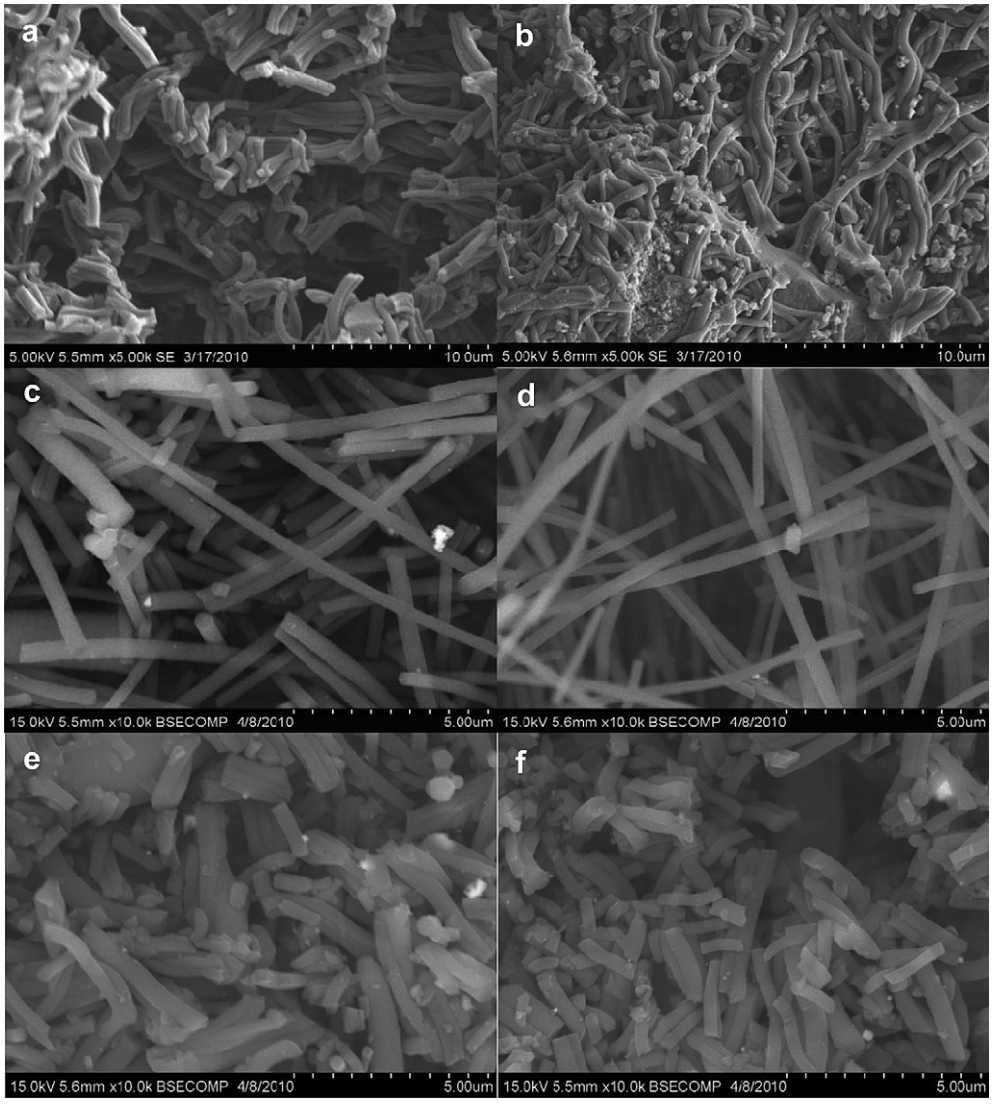

Fig. 10. SEM microstructures of the PNC fibers following the heating procedure in Table 1: (a) CF1, (b) MCF2, (c) MCF3, (d) MCF4, (e) MCF5 and (f) MCF6.

around the outer surface during shrinkage as the dehydrogenation and/or dehydrocyanide reaction proceeds.

The evolution of the fiber composition is further evidenced by the FT-IR spectra, Fig. 9. The gradually decrease in the intensities of the C≡N for saturated nitriles at 2240 cm^{-1} and the aliphatic C–H at 1453 cm^{-1} and 2922 cm^{-1} with increasing the heating temperature from 25 °C to 220 °C confirms the reactions of dehydrogenation and dehydrocyanide. With further increasing the heating temperature, these peaks disappear and several new peaks between 1200 and 1600 cm^{-1} are observed, Fig. 9d–f, indicating the growth of the C=C and C=N bands [60]. After annealing, the polymer fibers are converted to carbon fibers accompanied by the loss of the peaks in the typical range of 1000–1600 cm^{-1}, Fig. 9g.

3.5. Carbonization of the PAN/Fe@FeO PNC fibers

The stabilized PAN/Fe@FeO PNC fibers are subjected to further heating process under nitrogen with the aim to produce carbon nanocomposite fibers. Fig. 10 shows the carbon nanocomposite fibers after experiencing different stabilization and carbonization processes. These fibers can be classified into three groups based on the morphologies. Fig. 10a,b shows the wavy fibers bundled together and some unexpected debris is observed in Fig. 10b. Fig. 10c,d presents the well-separated straight carbon nanocomposite fibers with appreciable fiber length. Fig. 10e,f depicts the separated fibers in short length. The significant difference in the fiber morphology is majorly attributed to the stabilization time and temperature, carbonization time and temperature. The fiber bundling and fusion, Fig. 10a,b is probably due to the higher heating rate (25–280 °C within 1 h) and longer stabilization time (3.5 h). The high heating rate is able to introduce larger temperature gradient directing from central to surface, which inevitably brings larger inner stress inside the fiber. Finally, the fibers show wavy shaped structure and even bundle together to minimize the inner stress. With the elongation of the stabilization process, the dehydrogenation and dehydrocyanide reactions may happen not only on a single fiber, but also between the bundled fibers, and thus the "fusion" phenomenon is observed, Fig. 10a,b. By decreasing the heating rate (25–250 °C within 2 h), stabilization temperature (from 280 to 250 °C) and duration (from 3.5 to 1 h), the high quality carbon nanocomposite fibers with a diameter ~400 nm are obtained, Fig. 10c,d. Comparing with the results from MCF3 and MCF4, the carbonization temperature ranging from 600 to 800 °C does not show a significant effect on the fiber morphology. In other words, the stabilization process is the most prominent factor affecting the final morphology of the fibers. Enlightened from the above observations, it is reasonable to consider that the carbon nanocomposite fibers can be possibly chopped into small pieces with the help of the intensified thermal stress difference. Higher stabilization temperature (300 °C) with relatively longer duration time (2 h) is used to introduce larger thermal stress difference. As a result, short carbon nanocomposite fibers are observed, Fig. 10e,f.

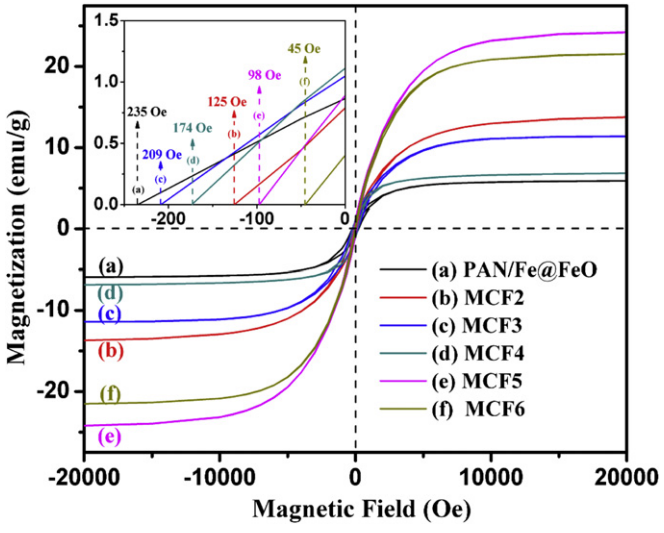

Fig. 11. Magnetic hysteresis loops of the electrospun PNC fibers and carbon nanocomposite fibers at room temperature.

3.6. Magnetic properties of the carbonized PAN/Fe@FeO PNC fibers

Fig. 11 shows the room temperature magnetic hysteresis loops of the electrospun PNC fibers and the PNC fibers after experiencing different stabilization and carbonization processes. The saturated magnetization (M_s) is 14.1, 6.8, 11.2, 21.5 and 24.1 emu/g for MCF2-MCF6, respectively, which is higher than 5.9 emu/g of the electrospun PAN/Fe@FeO fibers. The higher M_s of MCF5 and MCF6 can be partially justified considering that more iron oxide NPs had been reduced to iron NPs through the reduction reaction by carbonized polymer at higher carbonization temperatures. In addition, the less carbon residue after annealing at high temperatures also contributes to a higher magnetization based on the unit mass of the samples. The coercivity (H_c) is also related to the heating history on the fibers, as seen in the inset Fig. 11. The H_c of the pure Fe@FeO NPs is 62.3 Oe as reported previously [15]. The H_c of the electrospun PAN/Fe@FeO fibers is significantly enhanced to 235 Oe. This means that the NPs are magnetically harder after dispersing in the PAN fibers, which is primarily due to the decreased interparticle dipolar interaction arising from the enlarged NPs spacer distance for the single domain NPs [37,61,62] as compared to the closer contact of the pure NPs. After annealing, the H_c of the CF/Fe@FeO fibers decreased to 125, 174, 209, 45 and 98 Oe corresponding to the MCF2, MCF3, MCF4, MCF5 and MCF6, respectively, which is due to the decreased particle spacer distance arising from the fiber shrinkage during the carbonization.

4. Conclusion

Uniform and bead-free PAN fibers with different diameters are produced from various polymer solutions using electrospinning method. The fiber diameter is positively proportional to the polymer concentration. Fixing the PAN concentration at 10 wt%, the addition of different weight loadings of Fe@FeO NPs shows a negligible effect on the diameter of the PNC fibers. The morphology of the resulting fibers is correlated to the corresponding rheological behaviors of the pure PAN and PAN/Fe@FeO PNC solutions. The PNC fibers exhibit an enhanced thermal stability as compared to that of the pure PAN fibers owing to the confinement effect of the NPs. Magnetic carbon nanocomposite fibers are produced through the stabilization and carbonization of the electrospun PAN/Fe@FeO PNC fibers. The heating history including the stabilization and carbonization temperatures, stabilization time and carbonization time shows a significant effect on the carbon fiber morphology and the magnetic properties. The fiber stabilization process at different temperatures is monitored by FT-IR and the results indicate that 250 °C is enough to initiate the dehydrogenation and dehydrocyanide reactions while retaining the fiber morphology as evidenced by SEM. The carbonization temperature shows less effect on the fiber morphology. However, higher carbonization temperature and longer carbonization time generally cause larger saturated magnetization. Both short and long magnetic

carbon nanocomposite fibers can be simply produced by changing the heating procedure.

Acknowledgments

This project is financially supported by the Research Start-Up Grant and Research Enhancement Grant from Lamar University. We acknowledge the support from the National Science Foundation - Nanoscale Interdisciplinary Research Team and Materials Processing and Manufacturing (CMMI 10-30755) to obtain the DSC and TGA. D. P. Young acknowledges support from the NSF under Grant No. DMR 10-05764.

References

[1] Reneker DH, Yarin AL. Polymer 2008;49:2387–425.
[2] Zhu J, Wei S, Patil R, Rutman D, Kucknoor AS, Wang A, et al. Polymer 2011;52:1954–62.
[3] Huang ZM, Zhang YZ, Kotaki M, Ramakrishna S. Compos Sci Technol 2003;63:2223–53.
[4] Lai C, Guo Q, Wu X, Reneker DH, Hou H. Nanotechnology 2008;19:195303.
[5] Wang G, Ji Y, Huang X, Yang X, Gouma PI, Dudley M. J Phys Chem B 2006;110:23777–82.
[6] Chronakis IS. J Mater Process Technol 2005;167:283–93.
[7] Li D, Xia Y. Nano Lett 2003;3:555–60.
[8] Wang D, Li K, Teo WK. J Membr Sci 1996;115:85–108.
[9] Ma Z, Kotaki M, Ramakrishna S. J Membr Sci 2006;272:179–87.
[10] Shimizu Y, Okuno YI, Uryu K, Ohtsubo S, Watanabe A. Water Res 1996;30:2385–92.
[11] Krzysztof P, Njuguna J. Thermal degradation of polymeric materials. Shawbury, UK: Rapra Technology; 2005.
[12] Wind JD, Sirard SM, Paul DR, Green PF, Johnston KP, Koros WJ. Macromolecules 2003;36:6442–8.
[13] Zhu J, Wei S, Ryu J, Budhathoki M, Liang G, Guo Z. J Mater Chem 2010;20:4937–48.
[14] Zhu J, Wei S, Zhang L, Mao Y, Ryu J, Haldolaarachchige N, et al. J Mater Chem 2011;21:3952–9.
[15] Zhu J, Wei S, Chen X, Karki AB, Rutman D, Young DP, et al. J Phys Chem C 2010;114:8844–50.
[16] Cao X, Habibi Y, Lucia LA. J Mater Chem 2009;19:7137–45.
[17] Chen X, Wei S, Gunesoglu C, Zhu J, Southworth CS, Sun L, et al. Macromol Chem Phys 2010;211:1775–83.
[18] Zhu J, Wei S, Alexander M, Dang TD, Ho TC, Guo Z. Adv Funct Mater 2010;20:3076–84.
[19] Zhu J, Feng X, Shi Y, Wang H, Lu X. J Nanosci Nanotechnol 2009;9:5958–65.
[20] Zhou Z, Lai C, Zhang L, Qian Y, Hou H, Reneker DH, et al. Polymer 2009;50:2999–3006.
[21] Kim C, Choi YO, Lee WJ, Yang KS. Electrochim Acta 2004;50:883–7.
[22] Suzuki M. Carbon 1994;32:577–86.
[23] Endo M, Kim C, Nishimura K, Fujino T, Miyashita K. Carbon 2000;38:183–97.
[24] Steigerwalt ES, Deluga GA, Lukehart CM. J Phys Chem B 2002;106:760–6.
[25] Morgan PE. Carbon fibers and their composites carbon fibers and their composites. Boca Raton, FL: CRC Press; 2005. 185–267.
[26] Morita M, Nishimura N, Matsuda Y. Electrochim Acta 1993;38:1721–6.
[27] Teo WE, Ramakrishna S. Nanotechnology 2006;17:R89–106.
[28] Dai H, Gong J, Kim H, Lee D. Nanotechnology 2002;13:674–7.
[29] Shao C, Kim HY, Gong J, Ding B, Lee DR, Park SJ. Mater Lett 2003;57:1579–84.
[30] Viswanathamurthi P, Bhattarai N, Kim HY, Lee DR, Kim SR, Morris MA. Chem Phys Lett 2003;374:79–84.
[31] Guan H, Shao C, Chen B, Gong J, Yang X. Inorg Chem Commun 2003;6:1409–11.
[32] Ugaz VM, Cinader DK, Burghardt WR. Macromolecules 1997;30:1527–30.
[33] Zhu J, Wei S, Yadav A, Guo Z. Polymer 2010;51:2643–51.
[34] Rittigstein P, Priestley RD, Broadbelt LJ, Torkelson JM. Nat Mater 2007;6:278–82.
[35] Tuteja A, Duxbury PM, Mackay ME. Macromolecules 2007;40:9427–34.
[36] Mackay ME, Dao TT, Tuteja A, Ho DL, Van Horn B, Kim HC, et al. Nat Mater 2003;2:762–6.
[37] Zhang D, Karki AB, Rutman D, Young DP, Wang A, Cocke D, et al. Polymer 2009;50:4189–98.
[38] Grabowski DA, Schmidt C. Macromolecules 1994;27:2632–4.
[39] Deitzel JM, Kleinmeyer J, Harris D, Beck Tan NC. Polymer 2001;42:261–72.
[40] Chen DR, Pui DYH, Kaufman SL. J Aerosol Sci 1995;26:963–77.
[41] Li D, Xia Y. Adv Mater 2004;16:1151–70.
[42] Ji L, Saquing C, Khan SA, Zhang X. Nanotechnology 2008;19:085605.
[43] Zhang W, Wang Y, Sun C. J Polym Res 2007;14:467–74.
[44] Baumgarten PK. J Colloid Interface Sci 1971;36:71–9.
[45] Doshi J, Reneker DH. J Electrostat 1995;35:151–60.
[46] Reneker D, Yarin A, Fong H, Koombhongse S. J Appl Phys 2000;87:4531–47.
[47] Thompson CJ, Chase GG, Yarin AL, Reneker DH. Polymer 2007;48:6913–22.
[48] Silverstein RM, Webster FX, Kiemle D. Spectrometric identification of organic compounds. Hoboken: John Wiley and Sons, inc.; 2005.
[49] Mathur RB, Bahl OP, Sivaram P. Curr Sci 1992;62:662–9.
[50] Minagawa M, Miyano K, Takahashi M, Yoshii F. Macromolecules 1988;21:2387–91.
[51] Liang CY, Krimm S. J Polym Sci 1958;31:513.
[52] De P, Sathyanarayana DN, Sadasivamurthy P, Sridhar S. Eur Polym J 2002;38:847–55.
[53] De P, Sathyanarayana DN, Sadasivamurthy P, Sridhar S. Polymer 2001;42:8587–93.
[54] Sahiner N, Pekel N, Güven O. React Funct Polym 1999;39:139–46.
[55] Bastow T, Hardin SG, Turney TW. J Mater Sci 1991;26:1443–53.
[56] Yu T, Lin J, Xu J, Chen T, Lin S, Tian X. Compos Sci Technol 2007;67:3219–25.
[57] Kim HS. J Polym Sci B 1996;34:1181–6.
[58] Sivy GT, Gordon Iii B, Coleman MM. Carbon 1983;21:573–8.
[59] Badawy SM, Dessouki AM. J Phys Chem B 2003;107:11273–9.
[60] Usami T, Itoh T, Ohtani H, Tsuge S. Macromolecules 1990;23:2460–5.
[61] Guo Z, Lei K, Li Y, Ng HW, Prikhodko S, Hahn HT. Compos Sci Technol 2008;68:1513–20.
[62] Guo Z, Lin H, Karki AB, Wei S, Young DP, Park S, et al. Compos Sci Technol 2008;68:2551–6.